Unmanned Systems, Vol. 14, No. 4 (2026) 787–800

DOI: 10.1142/S2301385026500196

UNMANNED SYSTEMS
https://www.worldscientific.com/worldscinet/us

A Risk-Aware Obstacle Avoidance Path Planning Method for Unmanned Delivery Aerial Vehicles Under Urban Environment

Wenjie Liu [*,†], Chao Yang [*], Weida Wang [*,†,‡],
Tianqi Qie [*], Changle Xiang [*]

[*]*School of Mechanical Engineering, Beijing Institute of Technology, Beijing, P. R. China*

[†]*Yangtze Delta Region Academy of Beijing Institute of Technology, Jiaxing, P. R. China*

Path planning plays an important role in autonomous flight in the complex urban environment to achieve goods delivery tasks. Besides dense obstacles, the wall effect near tall buildings brings great risks to the unmanned delivery aerial vehicle (UDAV). The objective of this work is to mitigate the risks and improve the safety and reliability of the UDAV. Motivated by this objective, a risk-aware obstacle avoidance path planning method for UDAV is proposed. First, the model of ducted fan-type UDAV is introduced. By analyzing its driving environment, different kinds of risks, including the wall effect, are constructed as an urban risk map, which reduces computational complexity by mapping them from three-dimensional space to two-dimensional planes. Then, a risk-aware improved artificial potential field (APF) path planning method is proposed, with a precognitive architecture, to plan a feasible path avoiding risks. The infeasible problems of the traditional APF method are solved by adding pre-decision-making instruction and continuous actions. Finally, scenarios are built to verify the effectiveness of the proposed method. Results show that the proposed method can plan a safe path in a complex urban environment. Compared to the planned path proposed by the popular particle swarm optimization method and the APF method, the risk index is decreased by 16.25% and 14.10%, respectively.

Keywords: Unmanned aerial vehicle; risk assessment; artificial potential field; path planning; collision avoidance.

1. Introduction

Currently, rapid societal development has led to a surge in the number of ground vehicles, exacerbating traffic congestion. To alleviate this issue, urban air mobility (UAM) has emerged as one of the primary solutions [1]. Ducted fan-type unmanned aerial vehicle (UAV), which has the electric vertical take-off and landing (eVTOL) ability, has received lots of attention due to its high flexibility and mobility [2]. At the same time, it has a relatively small rotor plane with large thrust which is more flexible in the limited space and has a superior ability to maximize payload capacity [3]. With the above advantages, ducted fan type UAV is especially widely used in urban goods delivery as an unmanned delivery aerial vehicle (UDAV). The UDAV can carry goods and fly to the target point directly with low-cost, energy-saving and fast delivery. Meanwhile, with the progress of aviation and intelligent transportation technology, autonomous and intelligent flight of UDAVs performs better and better [4]. Path planning is a significant and fundamental issue for the autonomous delivery task [5]. It requires overcoming various challenges, such as dense obstacles and high dimensional space, as well as dynamic planning for emergencies [6].

Received 4 September 2024; Accepted 11 February 2025; Published 28 June 2025. This paper was recommended for publication in its revised form by editorial board member, Wei Meng.
Email Addresses: [‡]wangwd0430@163.com
[‡]Corresponding author.

A variety of works have been explored and studied on path planning [7]. And they can be divided into planning methods and reacting methods [8]. The planning methods generate feasible or even optimal paths ahead of time. Like the graph search planning method, the environment is represented as the grid map where the agent traverses the whole map with its heuristic function to find an optimal path in the A* method [9]. Sparse A* search method further combines the UAV maneuverability with the A* method and generates the flyable route for mission space [10]. The numerical optimization method can better combine with the platform, which formulates the specific landing task as a sequential convex programming problem [11]. To face the complex environment, the multi-objective swarm intelligence algorithm belonging to the numerical optimization method finds the optimal path under the terrain threat constraints through iterative optimization [12]. To face the environmental constraints, the model predictive control method could plan paths subject to state and control constraints [13]. The numerical optimization method could plan paths flexibly and exhibit high adaptability in a complex urban environment [14]. Reacting methods are equipped with an online collision avoidance system to respond to dynamic planning scenarios. Rapidly Exploring the Random Tree method could find the path effectively through incremental search. While it is limited to the high-dimensional domain and its planning efficiency. Existing works are mainly aimed at the dense obstacles. The artificial potential field (APF) method offers an elegant solution by building an APF to attract the agent toward the target position and to repel it away from the obstacles [15]. APF method is often used for path planning based on its flexible potential field establishment with low computational complexity [16–18]. The principle determines that the APF method can meet the requirements for collision avoidance in high-dimensional and dynamic environments [19]. At the same time, the potential field establishment can be combined with the risk of the environment naturally [20]. Above all, the APF method is a proposed way to achieve the goods delivery task in the urban environment.

Based on the above analysis, there are still some challenging tasks for UDAV path planning. First, the dense obstacles like tall buildings, trees and other structures make the UDAV more difficult to find feasible paths and more likely to fall into a local minimum. Second, the wall effect caused by the common tall buildings in the urban environment poses significant risks to the ducted fan type UDAV [21]. Planning methods that fail to account for this risk may lead to the UDAV being positioned too close to the building plane, resulting in instability. Third, as the UDAV may crash into pedestrians and vehicles on the ground, the risks including potential hazards during the driving task are equally important to take into consideration [22]. The problem addressed in this paper is to navigate around dense aerial obstacles and account for various risks, including the surrounding wall effect and potential ground-level hazards. Motivated by this issue, a risk-aware path-planning method for UDAVs in urban environments is proposed.

The main contributions of this work are as follows:

(i) A risk-aware path planning method for the UDAV is proposed, which is effective in facing the complex and dynamic urban environment.
(ii) An urban risk map is established to construct different risks, including the wall effect, and reduce computational complexity by mapping from three-dimensional space to two-dimensional planes.
(iii) The precognitive architecture is constructed to solve infeasible problems by adding pre-decision-making instruction and continuous actions.

The remainder of this paper is organized as follows. The UDAV model and urban risk map are introduced in Sec. 2. The risk-aware path planning method is proposed in Sec. 3. The experimental results and discussions are presented in Sec. 4. Section 5 concludes.

2. Modelling of UDAV and Urban Environment

In this section, UDAV and its driving environment are introduced. The ducted fan UDAV is described. With concerns about the complex dynamic urban environment, different risks are analyzed and modeled as an urban risk map which can be integrated into the risk-aware path planning method for UDAV.

2.1. *UDAV system description*

In this paper, a ducted fan-type UDAV is studied. The UDAV platform is a symmetric structure. The aerodynamic layout of UDAV is shown in Fig. 1.

The UDAV includes two main ducted fan systems and four auxiliary ducted fan systems. Each ducted fan system is powered by an independent drive electric motor which makes a great effort to ensure high efficiency and control flexibility of UDAV. The ducted fan system with its drive electric motor comprises each lift unit of the lift system. The control system regulates the motion of the UDAV by adjusting the rotation speed of each lift unit. The power of UDAV is provided by the electric propulsion system which is built into the propulsion system cabin. With the high efficiency of the propulsion system, the platform can support heavy payload and extend the operation range. Goods are delivered through a mechanical fixed connection to a mechanical interface located under the propulsion system cabin. The parameters of the UDAV platform are as shown in Table 1.

Having the ability to hover and adjust attitude in place, the UDAV can fly point-to-point and consider the path. The

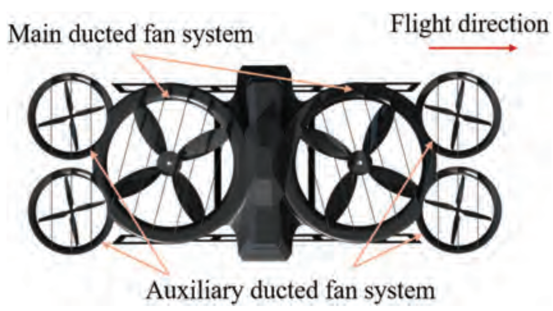

(a)

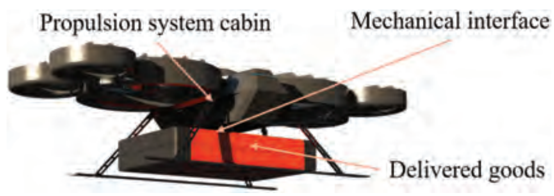

(b)

Fig. 1. The diagram of the UDAV. (a) The aerodynamic layout of UDAV. (b) The connection between UDAV and delivery goods.

Table 1. Parameters of the UDAV.

Parameters	Value
Mass (with Payload)	630 kg
Length × Width × Height	6 m × 2 m × 1.5 m
The radius of Main Ducted Fan	1.9 m
Radius of Auxiliary Ducted Fan	0.9 m

world frame and body frame are used to express the motion of the UDAV. The position vector p_b and the attitude angle vector Φ_b of the UDAV of the body frame can be written as

$$\begin{cases} p_b = [x \quad y \quad z]^T, \\ \Phi_b = [\varphi \quad \theta \quad \psi]^T, \end{cases} \tag{1}$$

where x, y, z are longitudinal, lateral and altitude positions of the UDAV, respectively. φ, θ, ψ are the yaw angle, pitch angle and roll angle of the UDAV, respectively.

The rotation matrix between the world frame and body frame can be written as

$$R_b = \begin{bmatrix} c_\psi c_\theta & c_\psi s_\theta s_\varphi - s_\psi c_\varphi & c_\psi s_\theta c_\varphi + s_\psi s_\varphi \\ s_\psi c_\theta & s_\psi s_\theta s_\varphi + c_\psi c_\varphi & s_\psi s_\theta c_\varphi - c_\psi s_\varphi \\ -s_\theta & c_\theta s_\varphi & c_\theta c_\varphi \end{bmatrix}, \tag{2}$$

where s_Δ and c_Δ are $\sin\Delta$ and $\cos\Delta$, respectively. Δ is the indicator of the attitude angle φ, θ and ψ, respectively. The coordinate system conversion equation between the world frame and body frame is written as

$$p_w = R_b p_b. \tag{3}$$

The motion information of the UDAV can be expressed in the world frame through the above coordinate system conversion and is abbreviated as X. With the armed sensors of the UDAV, the environment information and the motion of the platform are obtained. To simplify the expression of the UDAV and driving environment, the following description is uniformly presented in the world frame.

2.2. *Urban risk map*

The goods delivery task for UDAV in the urban environment requires careful planning to avoid collisions with common buildings or other structures. For the ducted fan type, the aerodynamic interference is also non-negligible for steady and safe flight. Thus, the wall effect caused by the near-constraint surface of tall buildings, hanging structures, or other confined environments should be considered seriously. Besides, third-party risk issues are also under consideration, including potential hazards to the vehicles and pedestrians on the ground.

As shown in Fig. 2, the above risk elements of a low-altitude urban environment will influence the safe and stable flight of the UDAV. Considering the above risk elements of the urban environment, the influence of different risk elements of the 3D environment mentioned above is analyzed. An urban risk map is built based on constructing assessment functions of the above three risk categories.

(1) Direct crash risk

First, obstacles are modeled as a 3D map including the size of obstacles and obstacle position.

$$X_{\rm Obs} = (x_{\rm Obs}, y_{\rm Obs}, z_{\rm Obs}), \tag{4}$$

where $X_{\rm Obs}$ is position coordinate $(x_{\rm Obs}, y_{\rm Obs}, z_{\rm Obs})$ of the surface of the obstacle. Obs is the index of obstacles. The position and distance between the UDAV and obstacles can be obtained through the map and sensors.

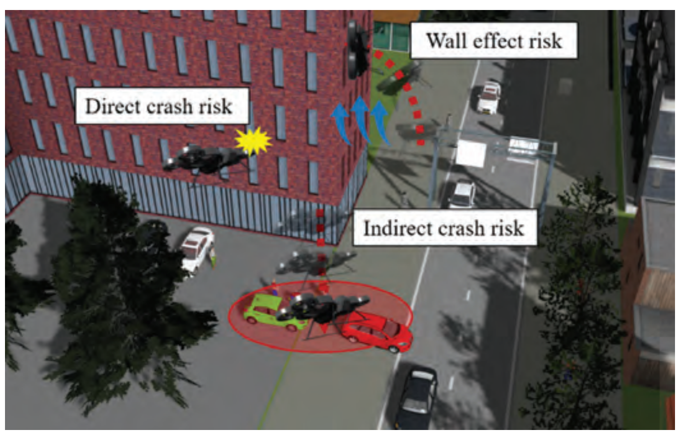

Fig. 2. Influence ways of different risk elements.

Then, for the dynamic obstacles like other UAVs under the driving environment, X_{Obs} can be represented as an ellipsoid model:

$$\frac{(x_{\text{Obs}}-x_o)^2}{(\frac{l_{\text{Obs}}}{2})^2}+\frac{(y_{\text{Obs}}-y_o)^2}{(\frac{w_{\text{Obs}}}{2})^2}+\frac{(z_{\text{Obs}}-z_o)^2}{(\frac{h_{\text{Obs}}}{2})^2}=1, \quad (5)$$

where $(x_{\text{Obs}}, y_{\text{Obs}}, z_{\text{Obs}})$ is the point position of the obstacle ellipsoid model surface similar to Eq. (4). (x_o, y_o, z_o) is the obstacle geometric center. l_{Obs}, w_{Obs}, h_{Obs} are the length, width and height of the obstacle, respectively.

For the obstacles at different steps, the position sequence $\boldsymbol{X}_{\textbf{Obs}}$ of each obstacle is defined as follows.

$$\boldsymbol{X}_{\text{Obs}}=\{X_{\text{Obs}}^{k}, X_{\text{Obs}}^{k+1}, X_{\text{Obs}}^{k+2}, \dots, X_{\text{Obs}}^{k+N}\}, \quad (6)$$

where k is the step of the current state of the UDAV, N is the horizon of steps.

The uncertainty of risk factors, including dynamic obstacles in the air should be considered. To model the motion uncertainty of dynamic obstacles, the ellipsoid model is adjusted using the confocal quadratic surface as shown in Eq. (5).

$$\frac{(x_{\text{Obs}}-x_o)^2}{(\frac{l_{\text{Obs}}}{2})^2+\lambda}+\frac{(y_{\text{Obs}}-y_o)^2}{(\frac{w_{\text{Obs}}}{2})^2+\lambda}+\frac{\left(z_{\text{Obs}}-z_o\right)^2}{(\frac{h_{\text{Obs}}}{2})^2+\lambda}=1, \quad (7)$$

where $\lambda \geq -(\min\{l_{\text{Obs}}, w_{\text{Obs}}, h_{\text{Obs}}\})^2$ is a factor in quantifying motion uncertainty. The adjust factor λ is related to the motion of the obstacle. The positions of the obstacle at different steps in the sequence X_{Obs} updates with the same factor λ. The safe influence radius of the obstacle Obs is related to the λ.

(2) Wall effect risk

To establish the risk assessment model related to the wall effect of near-constraint surface, the obstacle information and impact caused by them should considered, as shown in Fig. 3. According to the computational fluid dynamics simulation analysis, there is a positive correlation between the flight steady flight area and the distance from UDAV to the near-constraint surface [23]. Safe influence radius R_{impact} of the obstacle Obs is calculated as follows:

$$R_{\text{Obs,impact}}=r_{\text{impact}}\cdot\left[1+\frac{e^{-|X-X_{\text{Obs}}|}}{(1+e^{-|X-X_{\text{Obs}}|})^2}\right], \quad (8)$$

where r_{impact} is the influence radius of different obstacles which is the multiple of ducted fan rotor radius. In particular, r_{impact} is mainly related to the surface sizes of the tall buildings and hanging structures. The safe influence radius of the obstacle Obs is related to the r_{impact} and the relative distance.

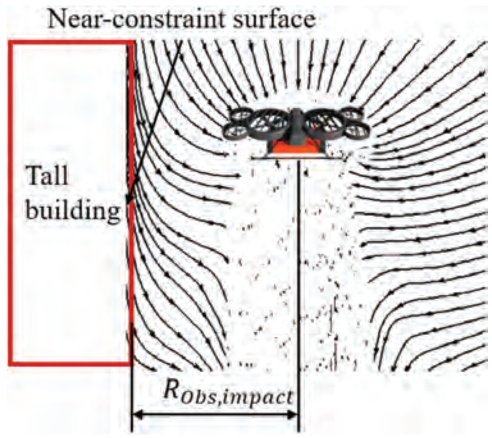

Fig. 3. Safe influence radius of wall effect.

(3) Indirect crash risk

The possibility of property damage can be also considered as follows;

$$X_{\text{Obs,impact}}=p_{\text{Obs,impact}}\cdot e^{-[(\frac{y-y_{\text{Obs},o}}{y_{\text{Obs,damp}}})^2+(\frac{z-z_{\text{Obs},o}}{z_{\text{Obs,damp}}})^2]}, \quad (9)$$

where $p_{\text{Obs,impact}}$ is a risk coefficient related to the shape and type of different risk elements. $y_{\text{Obs},o}$ and $z_{\text{Obs},o}$ are the parameters related to different risk elements. $y_{\text{Obs,damp}}$ and $z_{\text{Obs,damp}}$ are the parameters related to the size of risk elements.

Through the consideration of the above three risks, the urban risk map can be built based on the above risk assessment functions. Considering the UDAV cruises in the urban environment, the flight scene is updated based on the perception. The planning domain is reduced through mapping 3D space to 2D space which could reduce computational complexity due to the reduced dimensionality. The 3D space of the fight scene is divided into the XOY and YOZ planes to reduce computational complexity. In the XOY plane, the safe distance R_{IMP}^{k} at step k can be represented as follows:

$$R_{\text{IMP}}^{k}=\min(X^{k}, X_{\text{Obs}}^{k}), \quad \text{Obs}=1,\dots,n, \quad (10)$$

where $\text{Obs}=\{1,2,\dots,n\}$ is the index of obstacles of the environment. k is the step. X_{Obs}^{k} is calculated from the safe influence radius and the position of the obstacles. When the risk Obs belongs to the direct crash risk, the $R_{\text{Obs,impact}}$ is calculated through Eqs. (4), (5) and (7). When the risk Obs belongs to the wall effect risk, the $R_{\text{Obs,impact}}$ is calculated through Eq. (8). And at different steps, R_{IMP}^{k} between the UDAV and risk factor is shown in Fig. 4. T^{k} means different urban risk maps of XOY planes at step k.

In the YOZ plane, the risk map in front of the UDAV is built to indicate decision-making results. For the vertical plane of the urban environment scenario, the main factors are listed as follows: (1) obstacles in the air include tall buildings, signboards and dynamic obstacles. (2) the wall

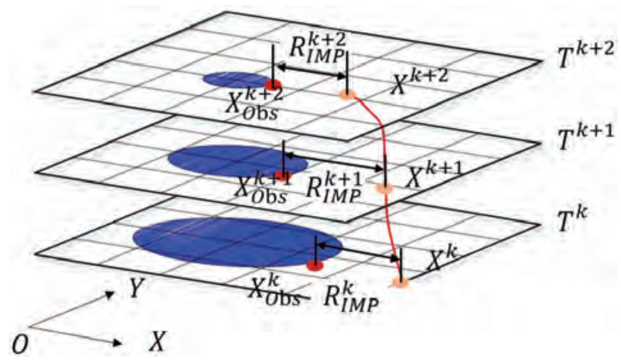

Fig. 4. Urban risk map of XOY plane.

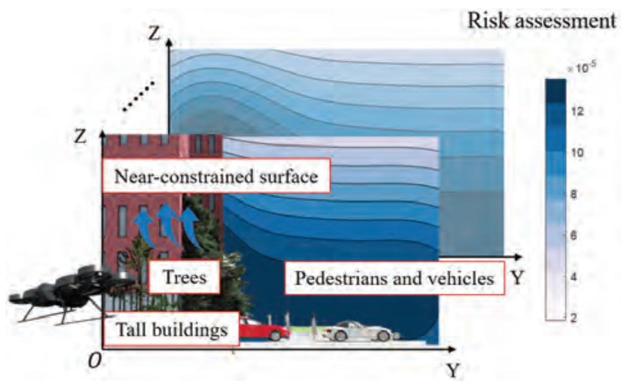

Fig. 5. Urban risk map of YOZ plane.

effect of tall buildings and signboards in the air. (3) possibility of property damage to the pedestrians and vehicles on the ground. To estimate the above elements quantitatively, an urban risk map in the YOZ plane related to the different positions along the x-axis is built, as shown in Fig. 5. The risk assessment value increases with the depth of the color.

Here, the relationship between the uncertainty and property damage is slight, and they are assumed to be independent. The risk map in the YOZ plane $P_{\mathrm{IMP}}(y,z)$ is described using the sum of the exponential functions of risk factors, which can be written as follows.

$$P_{\mathrm{IMP}}(y,z) = \sum_{\mathrm{Obs}=1}^{n} p_{\mathrm{Obs,impact}} \times e^{-[(\frac{y-y_{\mathrm{Obs}}}{y_{\mathrm{damp}}})^2+(\frac{z-z_{\mathrm{Obs}}}{z_{\mathrm{damp}}})^2]}. \tag{11}$$

3. Risk-Aware Path Planning Method for UDAV

In this section, a risk-aware path-planning method for UDAV is introduced. First, the APF path planning method is applied in the 3D urban environment based on the urban risk map. Next, the infeasible problems of the APF method are concluded in this part. Finally, to solve these problems and consider urban risks, the precognitive architecture is constructed to improve the effectiveness of the APF method.

3.1. *APF method based on the urban risk map*

In this part, taking the risk elements in the complex dynamic urban environment into consideration and solving the local minimum problem ensures flight safety. The urban risk map assesses the risks which can be used in this part. The UDAV drives in the APF under the effect produced by the repulsion potential field force from the obstacles and attractive potential field force from the target position. The definition of potential field is written as follows:

(1) Repulsion potential field.

Through the distance to the obstacle, the repulsion potential field U_{rep} is obtained as follows:

$$U_{\mathrm{rep}}(X_{\mathrm{Obs}}) = \begin{cases} \frac{1}{2}K_{\mathrm{rep}}\left(\frac{1}{|X-X_{\mathrm{Obs}}|} - \frac{1}{\rho_0}\right)^2, & |X-X_{\mathrm{Obs}}| \le \rho_0, \\ 0, & |X-X_{\mathrm{Obs}}| > \rho_0, \end{cases} \tag{12}$$

where K_{rep} is the repulsion factor. X is the current position of UDAV, X_{Obs} is the obstacle surface position. For the direct crash risk factor, X_{Obs} can be obtained from the map and sensors directly. For the dynamic UAV obstacles, their motion uncertainty risk factors are considered and the confocal quadratic surface position is used. ρ_0 is radius of influence which is different in the different risk elements. And for the tall building or other hanging structures, it is equal to the safe influence radius $\mathrm{R}_{\mathrm{Obs,impact}}$. According to the repulsion potential field, the repulsion potential field force is written as follows:

$$\begin{aligned} F_{\mathrm{rep}}(X_{\mathrm{Obs}}) &= -\nabla U_{\mathrm{rep}}(X_{\mathrm{Obs}}) \\ &= K_{\mathrm{rep}}\left(\frac{1}{|X-X_{\mathrm{Obs}}|} - \frac{1}{\rho_0}\right) \\ &\quad \times \left(\frac{1}{(X-X_{\mathrm{Obs}})^2} \cdot \frac{\partial(X-X_{\mathrm{Obs}})}{\partial X}\right), \\ &\quad |X-X_{\mathrm{Obs}}| \le \rho_0. \end{aligned} \tag{13}$$

(2) Attraction potential field.

Through the distance to the target position of the current driving goal, attraction potential field force is obtained.

$$U_{\mathrm{att}} = K_{\mathrm{att}} \cdot (X - X_G)^2, \tag{14}$$

where K_{att} is the attraction factor. X_G is the goal position. According to the attraction potential field, the attractive potential field force is written as follows:

$$F_{\text{att}} = -\nabla U_{\text{att}} = -2K_{\text{att}}(|X - X_G|)\frac{\partial(X - X_G)}{\partial X}. \quad (15)$$

The total potential field force F_{total} is the vector sum of the repulsion potential field and the attraction potential field.

Through two types of forces in different steps, the UDAV can realize obstacle avoidance in real time. The total potential field force F^k_{total} at step k and the UDAV position updating equation can be written as follows.

$$F^k_{\text{total}} = \sum F^k_{\text{rep}}(X_{\text{Obs}}) + F^k_{\text{att}}, \quad (16)$$

$$X^{k+1} = X^k + \Delta s_l * \frac{F^k_{\text{total}}}{|F^k_{\text{total}}|}, \quad (17)$$

where F^k_{rep} and F^k_{att} are repulsive potential field force and attractive potential field force at step k, respectively. X^{k+1} is the UDAV position at step $k+1$. Δs_l is the length of the equidistant path waypoints.

3.2. *Risk-aware path planning method*

A risk-aware path solution is obtained through the APF method based on the urban risk map. The dense obstacles and wall effect risks make the agent easily fall into the local minimum problem which is intermittent and random. The precognitive architecture is used to solve the infeasible problem based on two key phases, pre-decision-making and continuous actions. Pre-decision-making gives high-level instruction to the agent triggered by the state of the UDAV and the environmental risks. Continuous actions are the mapping from the pre-decision-making results to the potential field forces. In this part, the proposed risk-aware path planning method can further enhance the performance of the APF method.

From the definition of APF, the potential field force is the gradient of the potential field related to the obstacle position. With the change of flight scenes, the minimum points of the potential field are mutable and the total potential field is easily changed in a continuous horizon. The path easily encounters infeasible problems which are shown in Fig. 6.

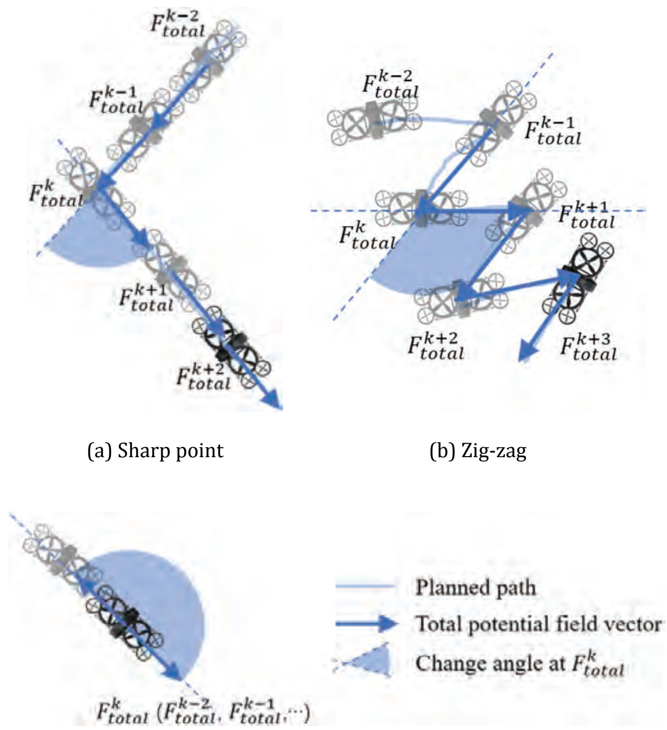

(a) Sharp point (b) Zig-zag

(c) Local minimum

Fig. 6. Problems of traditional APF. (a) A sudden change in the direction of the total potential field vector at different flight path positions. (b) Constant change of the direction of the total potential field vector at different flight path positions. (c) Nearly unchanged position of the flight path position and contrary potential field force vector.

Case 1. When the UDAV flies forward, the obstacle position of the flight scene changes immediately due to the different local minimum positions. Thus, there is a sudden change in the direction of the potential field vector at F^k_{total} at step k. The direction of previous vectors of the total potential field force and the follow-ups are usually consistent.

Similarly, when the UDAV is driving within a narrow passage of the total potential field, the planned path becomes zigzag and poorly feasible. The potential field force is oscillating within a small range along a direction. The direction of the potential field vectors is usually inversed in the other two directions.

The above situations can be concluded and detected by the change of potential field force direction of a different period with the above features.

$$\begin{cases} \theta(F^k_{\text{total}}, F^{k-1}_{\text{total}}, F^{\cdots}_{\text{total}}) < \varepsilon, \\ \theta(F^{k+\text{ind\_case}}_{\text{total}}, F^{k+\text{ind\_case}+1}_{\text{total}}, F^{\cdots}_{\text{total}}) < \varepsilon, \\ \theta_{i,j}(F^{\text{step\_case}}_{\text{total}}, F^{\text{step\_case}+1}_{\text{total}}) > \theta_0, \end{cases} \quad (18)$$

where $\theta(*)$ is the angle between the adjacent potential field forces. i, j are the index of two out of three directions. step_case is the step when the traditional APF cannot find a way to target and be detected. step_case $\in [k, k + \text{ind\_case}]$. ind_case is the indication of the step of a different case. For the sharp point, ind_case $= 1$. For the zig-zag situation, ind_case > 1. ε is the included angle which should satisfy the steering limitation of the UDAV dynamic constraints. θ_0 is a constant related to the UDAV constraint.

Case 2. Similar to the zigzag problem, the UDAV falls into a local minimum, not a global minimum, within a step length.

The planning path is terminated, and the UDAV is trapped away from the target position. The direction of the potential field force is contrary in three directions, and the position of the UDAV is nearly static.

For the third case, it can be detected from the position of the UDAV directly and shown as follows:

$$\sum_{\text{step\_case}=k}^{\text{ind\_case}} X^{\text{step\_case}} \leq \Delta s_l * \text{amp}, \tag{19}$$

where step_case $\in [k, k + \text{ind\_case}]$, ind_case > 1. amp is the amplified index of the trapped area. Case 2 is triggered if Eq. (19) is satisfied for more than ind_case consecutive times.

The risk-aware path planning method is proposed to solve the above problems and fit the complex environment. Here, a cognitively explicable precognitive architecture is used for the trigged decision-making instruction and continuous APF planning in this paper. For the APF method, it is helpful to give the pre-decision-making instruction when the UDAV falls into the above traps.

Corresponding to the above three problems, the precognitive architecture is illustrated as Algorithm 1.

In the precognitive architecture, the safe distance $R^k_{\text{IMP}}(\text{Obs})$ according to the risk assessment model is used to update each repulsive potential field force of the current fight scene. The impact of urban risk factors is taken into consideration. At the same time, the decision-making based on the urban risk map happens at the iteration when the case detection is triggered. The details about solutions 1 and 2 are shown as follows.

Algorithm 1. Precognitive architecture of improved APF method.

for k = 1: iteration
  Update obstacles' position and current position of UDAV at step k.
  for j = 1: Obs
    Calculate the repulsion force $F_{\text{rep}}(X_{\text{Obs}})$ of the X^k_{Obs} at different safe distance $R^k_{\text{IMP}}(\text{Obs})$
  end
  if case 2 occurs
    Solution 2
  end
  Calculate the total potential field at current step, $F^k_{\text{total}} = \sum F^k_{\text{rep}}(X_{\text{Obs}}) + F^k_{\text{att}}$
  Update UDAV position X^{k+1}
  UDAV planning path $\mathbf{X} \leftarrow X^{k+1}$
end
if find **case 2** in the planned path **X** near the target point
  Solution 2
end
if find **case 1** in the planned path **X**
  Solution 1
end

Solution 1. For case 1, it is can be solved by the elastic band theory. Elastic band theory is a method used to calculate the path from one local minimum to another. Through adjusting its tension and shape to adjust the planned path when case 1 occurs. Here, solution 1 can be written as follows. J, J_1 and J_2 are the cost functions of this optimization, respectively. The path can be smooth without a sharp point and jitter through the optimization.

$$\begin{cases} \underset{X}{argmin} J = \sum_{\text{step\_case}=q}^{\text{opt\_case}-1} \|\alpha \cdot (J_1) + \beta \cdot (J_2)\|^2, \\ J_1 = X^{*,\text{step\_case}} - X^{\text{step\_case}}, \\ J_2 = X^{*,\text{step\_case}} - X^{*,\text{step\_case}+1}, \end{cases} \tag{20}$$

where q and opt_case are the endpoints of expanded range, respectively. For the sharp point, opt_case $= 2$. For the zigzag, opt_case > 2. $X^{*,\text{step\_case}}$ is the corresponding optimized path point of original path point $X^{\text{step\_case}}$. α and β are the adjusted parameters.

Solution 2. For the case 2, it can be solved based on the previous urban risk map mentioned in Sec. 2. In the flight scene, there are many obstacles, and the UDAV falls into the local minimum trap easily. In this case, a decision-making potential field force is added according to the urban risk map in the YOZ plane in Fig. 7.

The UDAV traps into local minimum because of the accumulation of multiple potential fields. Thus, the decision-making potential field force is produced according to the risk assessment using a different way and rebuild an additional attractive potential field. The decision-making potential field force which is shown in Fig. 7(b) is written as follows:

$$F^k_{\text{dm}}(y,z) = -\nabla P^k_{\text{IMP}}(y,z), k \in [k, k + \text{opt\_case}], \tag{21}$$

where F^k_{dm} is the decision-making force at step k. At the same step, the decision-making potential field force is the negative gradient of risk assessment in the YOZ plane. The decision-making potential field force is an additional potential field force to help the agent out of the current local minimum. By adding this force, the total potential field force can be written as follows:

$$F^k_{\text{total}} = \sum F^k_{\text{rep}}(X_{\text{Obs}}) + F^k_{\text{att}} + F^k_{\text{dm}}, \quad k \in [k, k + \text{opt\_case}]. \tag{22}$$

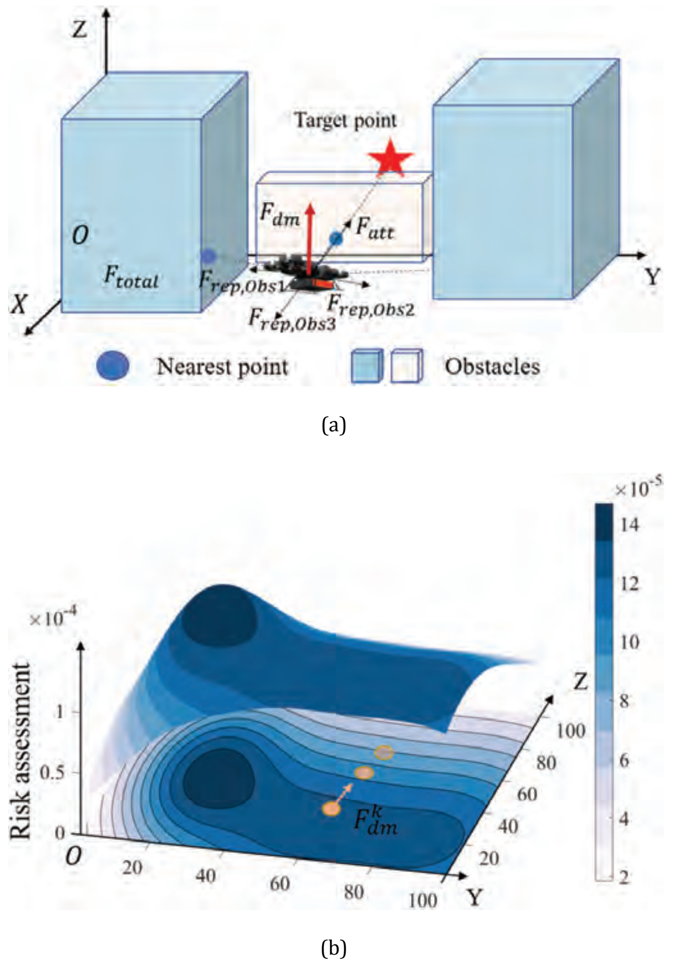

Fig. 7. Decision-making of urban risk map. (a) Schematic diagram of potential field force. (b) Urban risk map in YOZ plane.

4. Results and Discussion

In this section, the performance of the proposed method is evaluated. First, the comparison of the popular methods, the APF method, the APF method based on the urban risk map (APF-URM method) and the proposed method are provided. Second, different flight scenes are proposed to show the effective improvement of the proposed method.

4.1. *Comparison among different methods*

A flight scene is built to verify the effectiveness of the proposed method which is shown in Fig. 8. For the urban delivery task, there are some buildings and trees with varying shapes and sizes. The wall effect of the near-constrained surface is non-negligible which is shown by the several blue arrows.

To validate the proposed method in the above flight scene, the popular A* method [24] and particle swarm optimization (PSO) method [25] are widely used in path

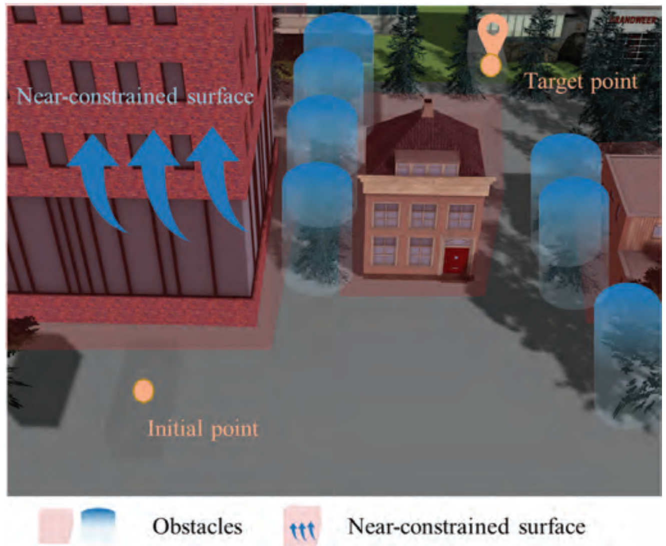

Fig. 8. Schematic diagram of flight scene.

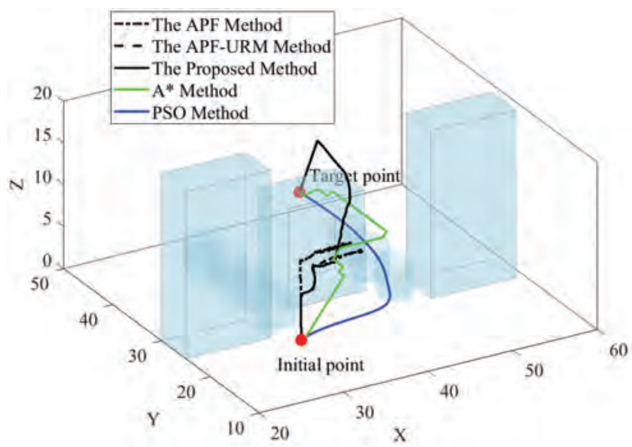

Fig. 9. Planning results of different methods.

planning. At the same time, the APF method and the APF-URM method are also applied to verify the effectiveness of the proposed method. The information of the flight scene is taken into consideration to plan the path. The involved parameters of the proposed method are set as follows. K_{rep} is 0.1. K_{att} is 0.06. Δs_l is 0.3. amp is 1.2. α and β are 0.5, respectively.

The planned paths of the five methods are shown in Fig. 9. The UDAV needs to avoid the middle building and reach at the target point under the effort of different methods. Starting from the initial point, the positions of all methods in the x-axis are increasing due to chasing the target point. The APF method, the APF-URM method, and the proposed method show faster rates of incensement in the y-axis. After about $y = 27$ m, there are huge differences in the different operations of the five planned paths. The planned path of

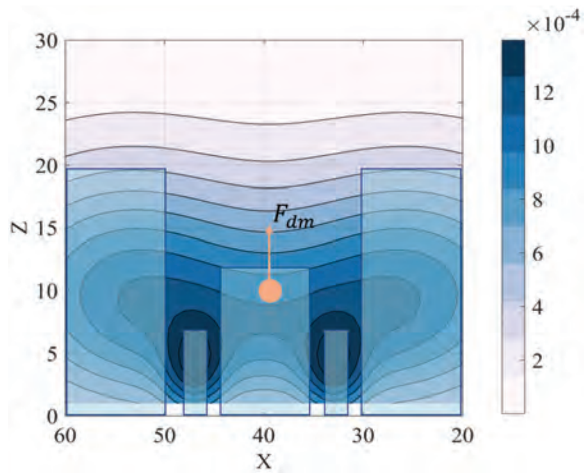

Fig. 10. The schematic diagram of the proposed method based on the urban risk map at position $y = 27$ m in the XOZ plane.

the A^* method and PSO method is still increasing the lateral position in the y-axis with a relatively small distance increment in the x-axis and z-axis. Especially for the A^* method, the planned path closely adheres to the boundaries of obstacles. Between $y = 27$ m and $y = 30$ m, the planned paths of the APF method and the APF-URM method have a long period oscillation along the x-axis direction from $x = 35$ m to $x = 43$ m and end at the position, not the target point. The planned path of the proposed method starts ascending at $x = 38$ m and climbs from $z = 5$ m to $z = 15$ m and ends at the target point.

Figures 10 and 11 show the improvement of the proposed method in solving typical problems of the APF method. When the UDAV falls into the local minimum position in front of the middle building, the decision-making potential field force is adopted to solve these cases. Under the effort, the planned path of the proposed method starts ascending and passes through the middle building. Figure 11 shows the effectiveness of the improvement.

To quantify the performance in driving safety, four indicators are designed, including feasibility, efficiency index (EI), safe index (SI) and risk index (RI). Feasibility means the planned path arrives at the target point and does not fall into the local minimum.

EI is defined as the length of the planned path which can measure the zigzag problem simultaneously.

$$\mathrm{EI} = \sum_{k=1}^{\text{iteration}} \|\mathrm{X}^{k+1} - \mathrm{X}^{k}\|_2. \tag{23}$$

SI is built considering the distance to the obstacle and distance to the target point and safety problem due to the target being nonreachable which is defined as follows:

$$\mathrm{SI} = e^{-0.01*(X^{\text{iteration}} - X_G)} * \min_k \|X^k - X_{\text{Obs}}\|_2, \tag{24}$$

where $k\epsilon(1, \text{iteration})$. The path feasible is considered as a penalty coefficient. When the UDAV ends at the position $\mathrm{X}^{\text{iteration}}$ and does not reach the target point, the SI will be very small even if the UDAV is far from the obstacles.

RI is defined as the risk cost of each path generated by methods. Given the location, size and impact range of obstacles in the environment, the RI of each position related to the different risk elements Obs is defined as follows:

$$\mathrm{RI}(k, \mathrm{Obs}) = \frac{1}{2\pi * R_{\text{Obs,impact}}} \times e^{-\frac{[(X^k - X^k_{\text{Obs}})^2]}{2*R^2_{\text{Obs,impact}}}}. \tag{25}$$

The risk of the position point is assumed to be satisfied a normal distribution. The mean value is set as the location of the risk element. The standard deviation is set as the impact radius of the element. The farther away the UDAV is from the risk element, the smaller the value of RI(k, Obs). The RI of

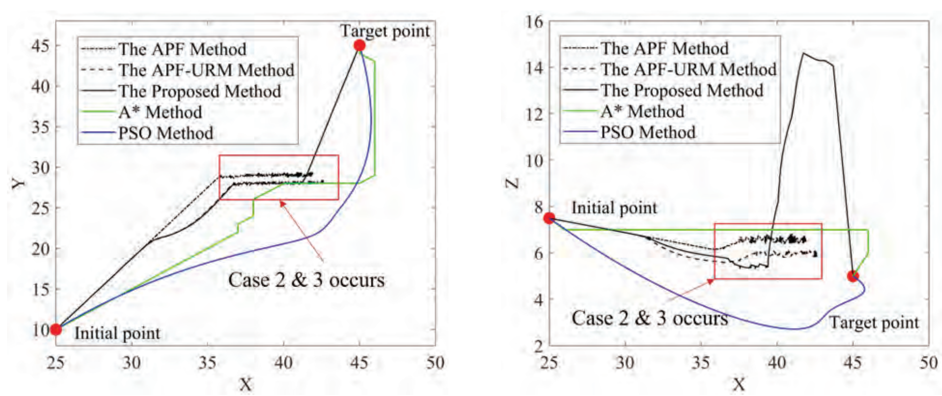

(a) (b)

Fig. 11. The improvement of the proposed method for solving typical problems of the APF method. (a) Planning results in the XOY plane and (b) Planning results in the XOZ plane.

Table 2. Performance of comparison methods.

Algorithm	Feasibility	EI	SI	RI
The proposed method	feasible	60.12	1.13	0.067
The APF-URM method	infeasible	170.88	0.002	0.068
The APF method	infeasible	166.18	0.001	0.078
A* method	feasible	47.86	1.01	0.070
PSO method	feasible	45.71	0.09	0.080

the planned path results can be written as follows:

$$\mathrm{RI} = \max \mathrm{RI}(k, \mathrm{Obs}). \quad (26)$$

The performance of the five methods is shown in Table 2.

From the performance comparison, the distance of the planned path proposed by the PSO method is the shortest with the lowest value of 45.71 m. The planned path by the A^* method is short with a value of 47.86 m with a low EI value while sacrificing safety with the smallest SI. Passing through the middle building brings more risk cost for the UDAV which is shown as the higher RI. The safest planned path is planned by the proposed method with the SI value of 1.13. The planned path proposed by the APF-URM method is relatively safer and has a smaller RI than the path proposed by the APF method due to the urban risk map. The proposed method can plan a feasible path and arrive at the target point at a relatively short distance with a value of 60.12 m. Compared to other methods, the planned path of the proposed method shows the advancement in its highest RI and SI. The proposed method sacrifices the EI compared to the popular PSO method and A* method due to the risk awareness. While compared to the shortest planned path proposed by the PSO method, the RI is decreased by 16.25%. Compared to the traditional APF method, the RI is decreased by 14.10% due to solving the local minimum problem.

4.2. *Comparison among different scenes*

In the urban flight scenes, the host UDAV carried out the package through the urban environment. First, safe flight needs to be ensured by considering these buildings, trees and other static obstacles. Second, the constant take-off movement of dynamic obstacles adds complexity to flight path planning, influencing safe flight. Third, the influence of the wall effect on these buildings should be considered to ensure safe and stable flight operations. Thus, typical flight scenes are built to test the performance of the APF method, the APF-URM method and the proposed method.

(1) Flight scene 1

Flight scene 1 is used to evaluate the capability of the proposed method when facing a moving obstacle in a dynamic environment. In this scene, the tall buildings are located on both sides of the road. The wall effect of the near-constraint surface is in front of the UDAV at the beginning. The dynamic flight is taking off vertically. The diagram of this flight scene is shown in Fig. 12.

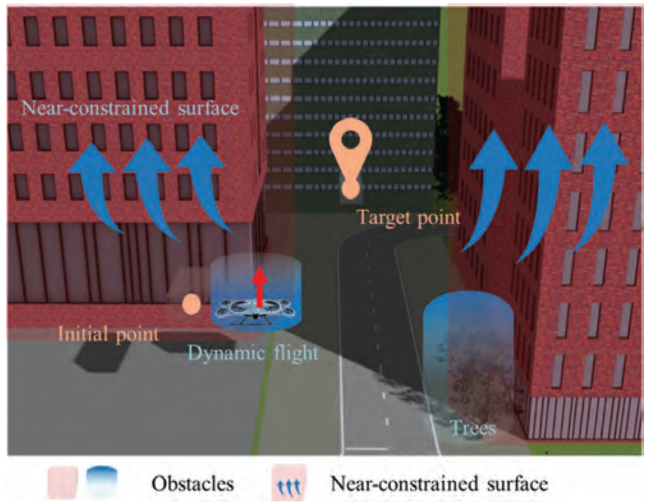

Fig. 12. Schematic diagram of flight scene 1.

In this flight scene, tall buildings and a dynamic flight are considered. The initial point is at $x = 25$ m and $y = 10$ m, with a height of 10 m. The dynamic flight lifts at $x = 30$ m and $y = 15$ m with an initial height of 7 m. The target point is in the middle of an open road to turn around at the next flight scene. The initial point and target point are shown as red points. Planning results are shown in Fig. 13.

In this scenario, the shape with the same color represents the same step. The dynamic flight is taking off around the initial point. Different line styles represent different planned paths of different methods which is the same as the previous setting. While for the clear distinction, the line colors are changed which is shown in the legend. The red dots are the initial point and target point, respectively. From the initial point, the longitudinal position of UDAV in the y-axis

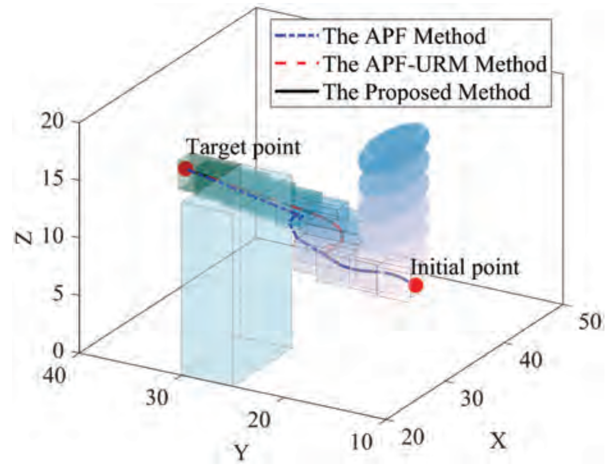

Fig. 13. Planning results of fight scene 1.

is increasing to the target point. After about $y = 12$ m, the UDAV starts to avoid the taking-off flight and yields to the left till around $y = 20$ m. The paths planned by the APF method involve direct flight toward the target points, with less pronounced evasive maneuvers. The planned paths of the APF-URM method and the proposed method have a period oscillation along the x-axis direction from $x = 27$ m to $x = 32$ m.

Through elastic band theory, the planned path using the proposed method is smooth without oscillation which dismisses the sharp point and zig-zag problem. By passing the building, the planned path of both methods is toward the target point under the attractive potential field force between $y = 21$ m and $y = 40$ m. Then, the planned paths using three methods all arrive at the target point in the end. The comparison between the above three methods is shown in Table 3.

From the planning results, the UDAV avoids taking off aircraft timely and drives around the building at a safe distance. The experimental results also show that the performance of the APF method can deal with dynamic obstacles in the driving environment. While for the APF method, there is the smallest SI and highest RI which represent a higher risk of the planned path. The consideration of the urban risk map can keep the UDAV away from obstacles. The potential field of the APF-URM is related higher at the building location when the dynamic obstacle lifting around $z = 10$ m.

Figure 14 shows the improvement of the proposed method for solving typical problems of the APF method. Through elastic band theory, the UDAV with the proposed method can solve the zigzag problem and make the flight path smooth with higher EI than the APF-URM method. While as the figure shows, the length of the planned path is sacrificed and with lower EI than the APF method. The SI of the planned path using the proposed method is also improved which is 4.30. Due to the similar steps, the reason for the decreased SI is minimum distance to the obstacle is increased by solving the zigzag case.

Table 3. Performance comparison.

Algorithm	Feasibility	EI	SI	RI
The Proposed method	feasible	36.88	4.30	0.007
The APF-URM method	feasible	38.21	4.25	0.008
The APF method	feasible	36.63	0.22	0.079

(2) Flight scene 2

During the flight, there is a broad traffic sign over the road. The tall buildings and trees are located on both sides of the road. The wall effect in this flight scene is also considered. Besides the above risk, there are some pedestrians and vehicles on the ground. The target point is located on the other side of the road which is a delivery station. To evaluate the capability when facing different risks, flight scene 2 is provided, shown in Fig. 15.

The different risk factors exist in this flight scene, and the UDAV keeps the different safe distances to the risk. And the dense obstacles surround the road which is necessary for the UDAV to cross. And the wall effect of the near-constrained surface on both sides of the road is considered. The planned path needs to consider the risk and plan a feasible path. Planning results by three methods are shown as follows.

The planned path of the three methods is shown in Fig. 16. From the initial point at $x = 25$ m and $y = 10$ m with a height of 5 m, the planned paths of the three methods are increasing in the x-axis and y-axis. Between $x = 30$ m and $x = 35$ m, the planned paths of the APF-URM method and the proposed methods are increasing faster in the x-axis. After around $x = 35$ m and $y = 28$ m, there is a long zigzag period along the x-axis direction between around $y = 27$ m and $y = 29$ m using the APF-URM method. The UDAV using

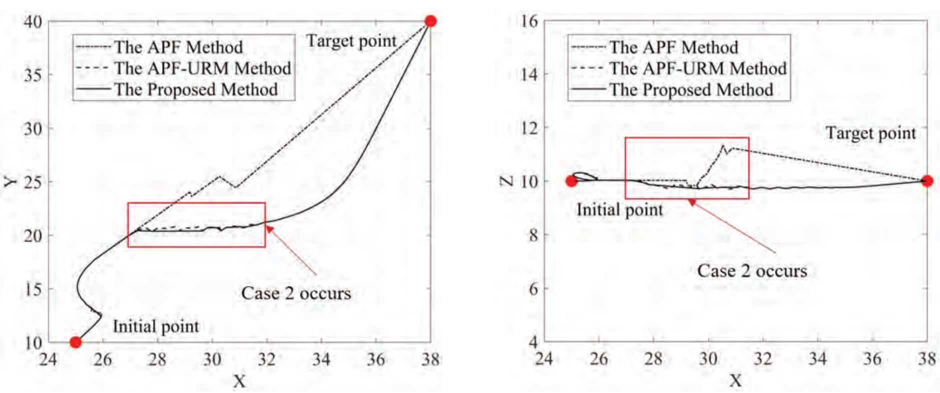

(a) (b)

Fig. 14. The improvement of the proposed method for solving typical problems of the APF method. (a) Planning results in XOY plane. (b) Planning results in XOZ plane.

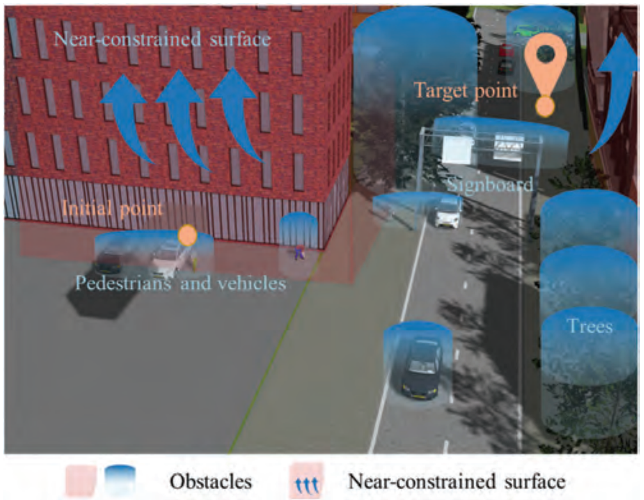

Fig. 15. Schematic diagram of flight scene 2.

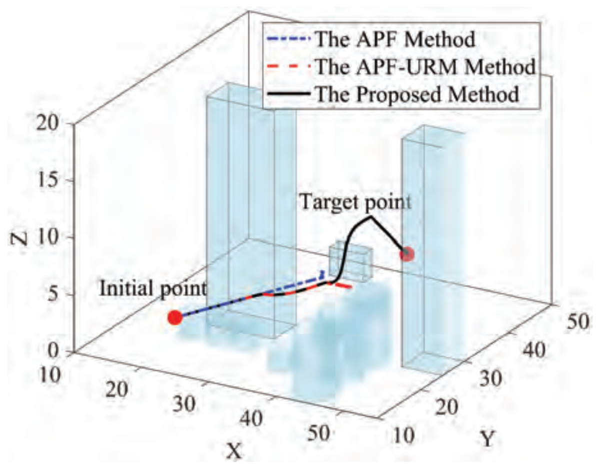

Fig. 16. Planning results of fight scene 2.

the APF method is falling into the local minimum at about $y = 28$ m. With the help of the decision-making potential field force, the planned path using the proposed method is smooth and upward to avoid obstacles at $x = 39$ m. The planned path using the proposed method is upward to the height of 9.89 m from $y = 27.80$ m to $y = 33.05$ m. And then it ends at the target point. The comparison between different methods is shown in Table 4.

From the experimental results, the planned paths of the APF method and APF-URM method are infeasible with poor EI, SI and RI. The planned paths using the APF method and

Table 4. Performance comparison.

Algorithm	Feasibility	EI	SI	RI
The Proposed method	feasible	41.81	1.892	0.050
The APF-URM method	infeasible	173.33	0.008	0.054
The APF method	infeasible	174.35	0.005	0.069

APF-URM method fall into a local minimum trap and oscillate around it. Due to the continuous oscillation and target nonreachable, the EI of the APF method and the APF-URM method is up to 174.35 m and 173.33 m, respectively. Due

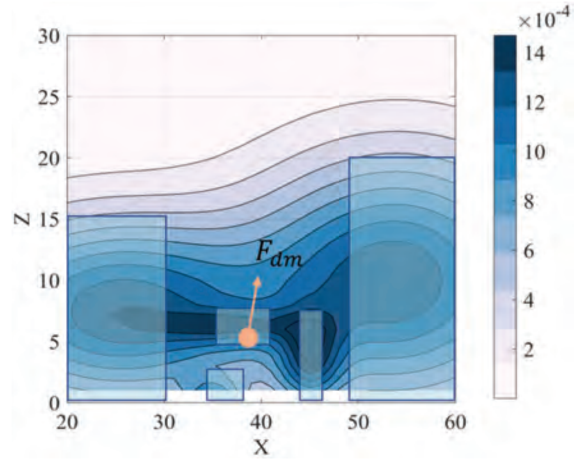

Fig. 17. The schematic diagram of the proposed method based on the urban risk map at position $y = 27.80$ m in the XOZ plane.

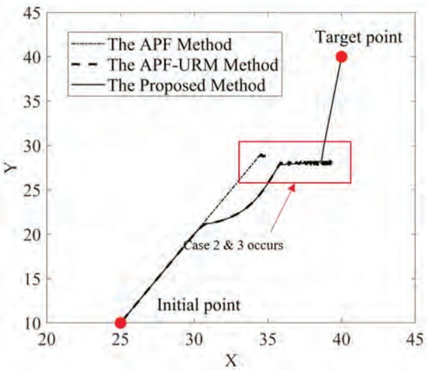

(a)

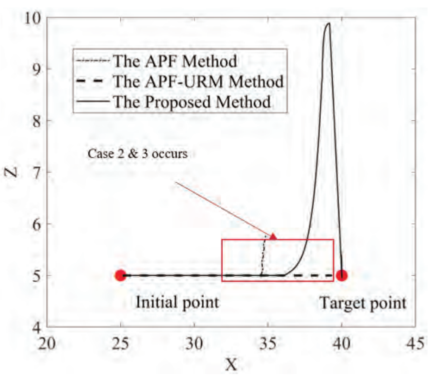

(b)

Fig. 18. The improvement of the proposed method for solving typical problems of the APF method. (a) Planning results in *the* XOY plane and (b) Planning results in *the* XOZ plane.

to the target nonreachable, the SI of the APF method and the APF-URM method are about 0.005 and 0.008 which indicates the unsafety of the planned paths. The decision-making potential field force is used to solve the local minimum case which is shown in Fig. 17. Through the decision-making potential field force, the SI using the proposed method is significantly improved. By adding the decision-making potential field force, the proposed method efficiently solves the local minimum.

The EI of the planned path proposed by the proposed method which is 41.81 m is clearly shorter than the APF method and APF-URM method. The RI of the APF method and the APF-URM method are about 0.069 and 0.054. The RI of the planned path using the proposed method is 0.050, indicating the lowest risk cost of the planned path. Figure 18 shows the improvement of the proposed method in solving typical problems of the APF method.

5. Conclusion

This paper proposes a risk-aware path-planning method for the UDAV in a complex dynamic urban environment. By constructing risk assessment functions, an urban risk map is built to consider risk elements of the environment including the wall effect. Based on the urban risk map, a risk-aware path planning method is proposed. Aiming to solving the infeasible problems of the traditional APF method, the precognitive architecture is constructed to plan a feasible and safe path. The validation shows improved performance of the proposed method. Compared to the planned path proposed by the popular PSO method and the APF method, the RI is decreased by 16.25% and 14.10%, respectively. From the experiment results, the proposed method demonstrates superior performance compared to the APF method and the APF-URM method in solving the local minimum and target nonreachable issues, thereby enabling the planning of feasible, safe and smooth paths in the complex dynamic environment. In future work, the proposed method will be related to the specific system performance and model uncertainty for the future application of the platform.

Declaration of Competing Interest

The authors declare that they have no known competing financial interests or personal relationships that could have appeared to influence the work reported in this paper.

Acknowledgment

This work was supported by the Natural Science Foundation of Chongqing, China under Grant CSTB2022NSCQ-MSX1056.

ORCID

Wenjie Liu
https://orcid.org/0000-0003-1327-0221
Chao Yang
https://orcid.org/0000-0001-9255-0752
Weida Wang
https://orcid.org/0000-0001-6420-5898
Tianqi Qie
https://orcid.org/0000-0002-3851-9890
Changle Xiang
https://orcid.org/0009-0002-5424-1670

References

[1] N. Swaminathan, S. R. P. Reddy, K. RajaShekara and K. S. Haran, Flying cars and eVTOLs—technology advancements, powertrain architectures, and design, *IEEE Trans. Transp. Electrific.* **8**(4) (2022) 4105–4117.

[2] H. Wei, B. Lou, Z. Zhang, B. Liang, F.-Y. Wang and C. Lv, Autonomous navigation for eVTOL: Review and future perspectives, *IEEE Trans. Intell. Veh.* **9**(2) (2024) 4145–4171.

[3] Y. Zhang, C. Xiang, B. Xu, Y. Wang and X. Wang, Design and implementation of a novel aerial manipulator with tandem ducted fans, in *Proc. 2018 IEEE/RSJ Int. Conf. on Intelligent Robots and Systems* (*IROS*) (2018).

[4] P. Wu, X. Yang, P. Wei and J. Chen, Safety assured online guidance with airborne separation for urban air mobility operations in uncertain environments, *IEEE Trans. Intell. Transp. Syst.* **23**(10) (2022) 19413–19427.

[5] W. Liu, T. Zhang, S. Huang and K. Li, A hybrid optimization framework for UAV reconnaissance mission planning, *Comput. Ind. Eng.* **173** (2022) 108653.

[6] J. Guo, W. Xia, X. Hu and H. Ma, Feedback RRT* algorithm for UAV path planning in a hostile environment, *Comput. Ind. Eng.* **174** (2022) 108771.

[7] X. Fu, C. Zhi and D. Wu, Obstacle avoidance and collision avoidance of UAV swarm based on improved VFH algorithm and information sharing strategy, *Comput. Ind. Eng.* **186** (2023) 109761.

[8] X. Yang and P. Wei, Autonomous free flight operations in urban air mobility with computational guidance and collision avoidance, *IEEE Trans. Intell. Transp. Syst.* **22**(9) (2021) 5962–5975.

[9] C. Li, X. Huang, J. Ding, K. Song and S. Lu, Global path planning based on a bidirectional alternating search A* algorithm for mobile robots, *Comput. Ind. Eng.* **168** (2022) 108123.

[10] R. J. Szczerba, P. Galkowski, I. S. Glickstein and N. Ternullo, Robust algorithm for real-time route planning, *IEEE Trans. Aerosp. Electron. Syst.* **36**(3) (2000) 869–878.

[11] Z. Shen, G. Zhou, H. Huang, C. Huang, Y. Wang and F.-Y. Wang, Convex optimization-based trajectory planning for quadrotors landing on aerial vehicle carriers, *IEEE Trans. Intell. Veh.* **9**(1) (2024) 138–150.

[12] Y. Wan, Y. Zhong, A. Ma and L. Zhang, An accurate UAV 3-d path planning method for disaster emergency response based on an improved multiobjective swarm intelligence algorithm, *IEEE Trans. Cybern.* **53**(4) (2023) 2658–2671.

[13] W. Zheng and B. Zhu, Control Lyapunov–Barrier function based model predictive control for stochastic nonlinear affine systems, *Int. J. Robust Nonlinear Control* **34**(1) (2023) 91–113.

[14] B. Zhu, X. Yuan, L. Dai and Z. Qiang, Finite-time stabilization for constrained discrete-time systems by using model predictive control, *IEEE/CAA J. Autom. Sin.* **11**(7) (2024) 1656–1666.

[15] O. Khatib, Real-time obstacle avoidance system for manipulators and mobile robots, *Int. J. Robot. Res.* **5**(1) (1986) 90–98.

[16] Z. Zuo, X. Yang, Z. Li, Y. Wang, Q. Han, L. Wang and X. Luo, MPC-based cooperative control strategy of path planning and trajectory tracking for intelligent vehicles, *IEEE Trans. Intell. Veh.* **6**(3) (2021) 513–522.

[17] H. Li, W. Liu, C. Yang, W. Wang, T. Qie and C. Xiang, An optimization-based path planning approach for autonomous vehicles using the dynEFWA-artificial potential field, *IEEE Trans. Intell. Veh.* **7**(2) (2022) 263–273.

[18] L. Li, J. Gan, X. Ji, X. Qu and B. Ran, Dynamic driving risk potential field model under the connected and automated vehicles environment and its application in car-following modeling, *IEEE Trans. Intell. Transp. Syst.* **23**(1) (2022) 122–141.

[19] Y. Shin and E. Kim, Hybrid path planning using positioning risk and artificial potential fields, *Aerosp. Sci. Technol.* **112** (2021) 106640.

[20] Z. Zhou, Y. Wang, G. Zhou, K. Nam, Z. Ji and C. Yin, A twisted gaussian risk model considering target vehicle longitudinal-lateral motion states for host vehicle trajectory planning, *IEEE Trans. Intell. Transp. Syst.* **24**(12) (2023) 13685–13697.

[21] Y. Luo, T. Ai, Y. He, Z. Zhao, B. Xu, Y. Qian, J. Peng and Y. Zhang, Aerodynamic analysis on unsteady characteristics of a ducted fan hovering in ceiling effect, *Eng. Appl. Comput. Fluid Mech.* **17**(1) (2023) 2196327.

[22] B. Pang, X. Hu, W. Dai and K. H. Low, UAV path optimization with an integrated cost assessment model considering third-party risks in metropolitan environments, *Reliab. Eng. Syst. Saf.* **222** (2022) 108399.

[23] T. Ai, C. Xiang, B. Xu, W. Fan and Y. Zhang, Influence of wall effect on comprehensive controllability for ducted fan aircraft, *J. Beijing Inst. Technol.* **29**(4) (2020) 581–591.

[24] S. Primatesta, G. Guglieri and A. Rizzo, A risk-aware path planning strategy for UAVs in urban environments, *J. Intell. Robot. Syst.* **95**(2) (2018) 629–643.

[25] V. Roberge, M. Tarbouchi and G. Labonte, Comparison of parallel genetic algorithm and particle swarm optimization for real-time UAV path planning, *IEEE Trans. Ind. Inform.* **9**(1) (2013) 132–141.

Wenjie Liu received her M.S. degree from the Beijing Institute of Technology, China, in 2022, respectively. She is currently working toward Ph.D. degree with the School of Mechanical Engineering, the Beijing Institute of Technology, Beijing, China.

Her research interests include decision-making and path planning for unmanned aerial vehicles.

Chao Yang (M’17) received his Ph.D. in Control Science and Engineering from the Yanshan University, Qinhuangdao, China, in 2016. From June 2012 to December 2015, he was working as a joint Ph.D. student (Supervisor: Dr. Liang Li), with Department of Automotive Engineering, the Tsinghua University, Beijing, China. From January 2016 to September 2018, he was working as a Postdoctoral Fellow, with the State Key Laboratory of Automotive Safety and Energy, Tsinghua University, Beijing, China. From April 2017 to April 2018, he was a visiting scholar at the University of Victoria, Victoria, B.C., Canada. He is currently an Associate Professor at the School of Mechanical Engineering, Beijing Institute of Technology, Beijing, China.

His research interests include advanced control theory and application on intelligent vehicles.

Weida Wang received the Ph.D. degree from the Beihang University, Beijing, China, in 2009. He is currently a Professor and the Vice Dean of the School of Mechanical Engineering, Beijing Institute of Technology, Beijing, China.

His current research interests include electric vehicles, automated vehicle motion planning and control, and electromechanical transmission control.

Tianqi Qie (Graduate Student Member, IEEE) received B.S. degree from the Beijing Institute of Technology, Beijing, China, in 2019. She is currently working toward Ph.D. with the School of Mechanical Engineering, Beijing Institute of Technology, Beijing, China.

Her research interests include vehicle trajectory prediction and decision-making for intelligent vehicles.

Changle Xiang received Ph.D. degree from the Beijing Institute of Technology, Beijing, China, in 2002. He is Honorary Professor with the Beijing Institute of Technology, and he is also the President of Dalian University of Technology. He has been elected as the Academician of the Chinese Academy of Engineering, Beijing, in 2019.

His research interests include vehicle dynamics and control, transmission control, and autonomous vehicle control.